



HAL
open science

An arbitrary-order immersed interface method for the two-dimensional propagation of acoustic and elastic waves

Roberto Sabatini, Alessandro Monti, Yan Pailhas, Angeliki Xenaki, Paul Cristini

► To cite this version:

Roberto Sabatini, Alessandro Monti, Yan Pailhas, Angeliki Xenaki, Paul Cristini. An arbitrary-order immersed interface method for the two-dimensional propagation of acoustic and elastic waves. *Physics of Fluids*, 2023, 35 (10), pp.107106. 10.1063/5.0167755 . hal-04292740

HAL Id: hal-04292740

<https://hal.science/hal-04292740>

Submitted on 17 Nov 2023

HAL is a multi-disciplinary open access archive for the deposit and dissemination of scientific research documents, whether they are published or not. The documents may come from teaching and research institutions in France or abroad, or from public or private research centers.

L'archive ouverte pluridisciplinaire **HAL**, est destinée au dépôt et à la diffusion de documents scientifiques de niveau recherche, publiés ou non, émanant des établissements d'enseignement et de recherche français ou étrangers, des laboratoires publics ou privés.

An arbitrary-order immersed interface method for the two-dimensional propagation of acoustic and elastic waves

Roberto Sabatini,¹ Alessandro Monti,² Yan Pailhas,² Angeliki Xenaki,² and Paul Cristini³

¹*Department of Physical Sciences and Center for Space and Atmospheric Research, Embry-Riddle Aeronautical University, Daytona Beach, Florida, USA*

²*NATO STO Centre for Maritime Research and Experimentation, La Spezia, Italy*

³*Aix-Marseille University, CNRS, Centrale Marseille, LMA, Marseille, France*

(*Electronic mail: yan.pailhas@cmre.nato.int)

(*Electronic mail: SABATINR@erau.edu)

(Dated: 17 July 2023)

This paper proposes an arbitrary-order immersed interface method for simulating the two-dimensional propagation of acoustic and elastic waves through fluid/solid interfaces. The present technique involves two main ingredients: 1) the linearized equations of continuum mechanics are simulated through an ADER (Arbitrary high-order schemes using DERivatives) scheme of arbitrary-order in both space and time (*J. Comput. Phys* **197**(2): 532–539, 2004); 2) the jump conditions along the material interfaces are taken into account through the “explicit simplified interface method” (ESIM) derived by Lombard and Piraux (*J. Comput. Phys* **195**(1): 90–116, 2004). In order to implement the ESIM, the computation of arbitrary-order spatial derivatives of the interface conditions is required. To this end, an algorithm for their numerical calculation, which does not require their explicit analytical expressions, is developed. Two numerical experiments involving flat and curved interfaces are finally discussed. When increasing the order of both the ADER scheme and of the interface treatment, the improvement of the convergence and of the accuracy of the numerical method is more specifically demonstrated by comparing the numerical results with analytical solutions.

I. INTRODUCTION

Simulating accurately the propagation of mechanical waves through heterogeneous media is essential in numerous scientific and engineering problems¹. In many physical applications, the propagation of acoustic and elastic waves is fairly well described by the linearized equations of continuum mechanics (LECM), *i.e.* the linearized Euler equations in fluids^{2,3} and the linear elastodynamic system in solids⁴. Finite-difference (FD) methods are widely employed for solving such partial differential equations (PDEs) in single material domains. They are indeed straightforward to implement, inherently well-suited for parallelization techniques⁵, and can reach very high accuracy^{6,7}. However, unlike finite-element methods⁸⁻¹³, FD schemes perform poorly in problems involving interfaces¹⁴, such as the seafloor in underwater acoustics or the surface of an object immersed in a fluid. Firstly, FD formulas are valid only for sufficiently smooth functions, while, along a boundary between media, the mechanical fields are generally discontinuous or even defined differently in different adjacent domains. Secondly, the wave variables must verify not only the LECM but also appropriate constraints² that are not incorporated in FD algorithms. Finally, FD methods are typically implemented on regular Cartesian grids. Consequently, an interface is implicitly represented as a series of stairs and steps, which generates spurious reflected and transmitted waves and degrades the quality of the numerical solution unless sufficiently small grid spacings are employed¹⁵. To sum up, without an adequate treatment of the interfaces, the reflection and the transmission of acoustic and elastic waves are generally not correctly described by FD algorithms.

To cope with these issues, one of the strategies proposed in the literature employs the immersed interface methods (IIMs)^{14,16-26}. Among the IIMs, two particular algorithms for solving the linearized equations of continuum mechanics deserve consideration: the IIM developed by Zhang and LeVeque¹⁶ and the method proposed by Lombard and Piraux¹⁴. In the former, the coefficients of the FD formula are modified near the interfaces to account for the aforesaid constraints, thereby maintaining an acceptable level of accuracy. In the latter, a unique FD scheme is instead employed in the whole computational domain, and ghost or modified variables are used where the FD stencil crosses a boundary. Both techniques allow for the geometrical features of the interfaces. The latter method is however more attractive for two main reasons: firstly, it exhibits higher numerical stability, which is indispensable in configurations involving materials with high contrasts of the physical parameters; secondly, unlike the Zhang's IIM, it can possibly reach arbitrary orders of accuracy. Nevertheless, despite its potential, current implementations of the latter IIM are only second- or fourth-order accurate. Unfortunately, high-quality numerical simulations often require a high resolution in terms of points-per-wavelength, especially when the number of grid points in the computational domain is limited, for instance by the GPU memory.

The core of the algorithm proposed by Lombard and Piraux¹⁴ lies in the computation of the ghost variables in the neighborhood of a boundary between media. The ghost variables are deduced from smooth extensions of the mechanical fields into the adjacent domains.

This calculation is performed through the “explicit simplified interface method” (ESIM), which requires high-order spatial derivatives of the interface constraints. More specifically, Lombard and co-authors argued, on the basis of the work carried out by Gustafsson²⁷, that conditions for the $(k - 1)^{\text{th}}$ -order derivative of the unknown field are needed for a FD scheme to retain k^{th} -order global accuracy^{20,21}. Unfortunately, deriving explicit expressions for such derivatives is an extremely tedious task, even for small values of k . For this reason, Lombard and Piraux¹⁴ suggested the use of symbolic calculus software.

This manuscript aims at elaborating a formally arbitrary-order generalization of the two-dimensional IIM proposed by Lombard and Piraux¹⁴, where the main novelty is the automatic computation of arbitrary-order spatial derivatives of the interface conditions. Specifically, the present method consists in the coupling of two main ingredients:

1. an ADER (Arbitrary high-order schemes using DERivatives) scheme of order s in both space and time^{28–30} to compute the numerical solution of the linearized equations of continuum mechanics;
2. a k^{th} -order ESIM for the treatment of the interfaces and the calculation of the ghost values in the neighborhood of material interfaces.

In order to simplify the forthcoming discussion, the proposed method is referred to as ADESIM $s - k$. The main contribution of this work is the development of a novel algorithm that calculates the arbitrary-order spatial derivatives of the interface conditions. Besides, although the ADER schemes were originally derived in the framework of the finite-volume method^{28–30}, a derivation based on finite differences is additionally carried out³¹. Finally, the proposed algorithm would be beneficial for the extension of the method to three-dimensional configurations as it allows the explicit calculation by hand of a high number of terms for the spatial derivatives of the interface conditions to be avoided (for instance, see the appendix in Lombard³²).

The paper is organized as follows. The physical problem, the governing equations, and the interface conditions are introduced in Section II. Section III is devoted to the development of the novel algorithm for calculating arbitrary-order spatial derivatives of the interface conditions. The ADESIM $s - k$ method is then described in Section IV. In Section V, two numerical experiments are discussed to assess the validity of the method. The improvement of the numerical accuracy when increasing the order of both the numerical scheme and of the interface treatment is more particularly examined by comparing the numerical results with analytical solutions. Specifically, the numerical tests will show a significant improvement of the accuracy for high values of $s - k$, e.g. $s = 6$ and $k = 5$, compared to the standard method with $s = 2$ and $k = 2$ ¹⁴. Concluding remarks are finally drawn in Section VI.

II. DESCRIPTION OF THE PHYSICAL PROBLEM

Introduce a Cartesian coordinate system Oxy and consider a generic interface Γ separating a fluid domain Ω_1 from a solid medium Ω_2 (cf. Figure 1). The curve Γ is described by a parameter τ as

$$\Gamma = \{(x(\tau), y(\tau)) \mid \tau \in \mathbb{I} \subseteq \mathbb{R}\}, \quad (1)$$

and its tangential and normal vectors, labeled as \mathbf{t} and \mathbf{n} , are defined by the expressions

$$\mathbf{t}(\tau) = \left[\frac{dx}{d\tau} \quad \frac{dy}{d\tau} \right]^T \quad \mathbf{n}(\tau) = \left[\frac{dy}{d\tau} \quad -\frac{dx}{d\tau} \right]^T \quad (2)$$

where the symbol T indicates the matrix transposition. The interface Γ is of class C^k , i.e. the functions $d^k x/d\tau^k$ and $d^k y/d\tau^k$ are everywhere continuous up to a order k .

In the study reported in this paper, the mechanical waves propagating through the media Ω_1 and Ω_2 are considered as small-amplitude perturbations of initial undisturbed ambient states (linearity assumption). The fluid ambient state is characterized by the density $\bar{\rho}_f$ and by the speed of sound \bar{c}_f . The acoustic propagation is described by the two components of the velocity perturbation \mathbf{u} , u_x^f and u_y^f , and by the pressure perturbation p , collected in the vector $\mathbf{U} = [u_x^f \quad u_y^f \quad p]^T$.

The physical parameters for the solid ambient state are the density $\bar{\rho}_s$, the speed of the P -waves \bar{c}_p and the speed of the S -waves \bar{c}_s , both expressed in terms of the Lamé coefficients, $\bar{\lambda}$ and $\bar{\mu}$ ³³, i.e. $\bar{c}_p = \sqrt{(\bar{\lambda} + 2\bar{\mu})/\bar{\rho}_s}$ and $\bar{c}_s = \sqrt{\bar{\mu}/\bar{\rho}_s}$. The elastic propagation is described by the two components of the elastic velocity \mathbf{u} , u_x^s and u_y^s , and by the three components of the elastic stress tensor Σ , σ_{xx} , σ_{xy} and σ_{yy} , collected in the vector $\mathbf{U} = [u_x^s \quad u_y^s \quad \sigma_{xx} \quad \sigma_{xy} \quad \sigma_{yy}]^T$. Along with the small perturbation hypothesis, the following premises are made:

- within each material domain, all ambient variables are independent of space and time;
- the fluid is at rest;
- the solid is isotropic and elastic;
- attenuation phenomena and body-force effects (such as the effect of gravity) are negligible.

Under these assumptions, the linearization of the equations of continuum mechanics leads to a first-order linear hyperbolic system^{3,4,14}:

$$\frac{\partial \mathbf{U}}{\partial t} = -\mathbf{A} \frac{\partial \mathbf{U}}{\partial x} - \mathbf{B} \frac{\partial \mathbf{U}}{\partial y}. \quad (3)$$

In Eq. (3), the matrices \mathbf{A} and \mathbf{B} are constant and depend on the physical parameters. The matrices are defined in a space $\mathbf{A}, \mathbf{B} \in \mathbb{R}^{3 \times 3}$ in the fluid, and $\mathbf{A}, \mathbf{B} \in \mathbb{R}^{5 \times 5}$ in the solid. Finally, for the mathematical problem to be well-posed, the following conditions must be additionally verified at a generic point P on the interface Γ and at each instant of time^{2,14}:

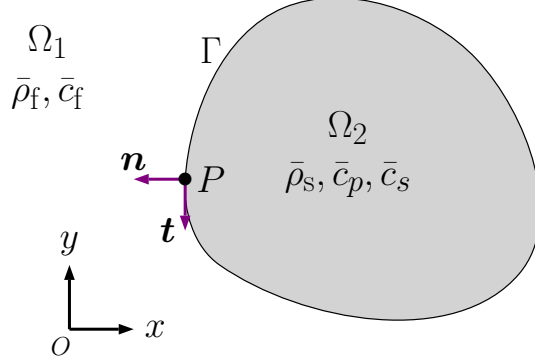


FIG. 1. (color online) Interface between a fluid Ω_1 and a solid Ω_2

- the normal velocity is continuous,

$$[[\mathbf{u}^T \mathbf{n}]] = 0, \quad \forall P \in \Gamma, \forall t; \quad (4a)$$

- the normal stress is continuous,

$$\mathbf{n}^T \Sigma \mathbf{n} = -p, \quad \forall P \in \Gamma, \forall t; \quad (4b)$$

- the tangential stress vanishes,

$$\mathbf{t}^T \Sigma \mathbf{n} = 0, \quad \forall P \in \Gamma, \forall t. \quad (4c)$$

III. ARBITRARY HIGH-ORDER INTERFACE CONSTRAINTS

In this section, the algorithm developed to compute arbitrary-order spatial derivatives of the interface conditions (4) is described. Such derivatives are employed in the ADESIM $s - k$ method presented in Sec. IV.

A. Notations

Consider a point P on Γ (cf. Figure 1). The limits of the solution $\mathbf{U}(x, y, t)$ and of its spatial derivatives up to the order k are collected in the vector

$$\mathbf{U}_i^k = \lim_{M \rightarrow P, M \in \Omega_i} \left[\mathbf{U}, \frac{\partial \mathbf{U}}{\partial x}, \frac{\partial \mathbf{U}}{\partial y}, \dots, \frac{\partial^\alpha \mathbf{U}}{\partial x^{\alpha-\beta} \partial y^\beta}, \dots, \frac{\partial^k \mathbf{U}}{\partial y^k} \right]^T, \quad \mathbf{i} = 1, 2, \quad \alpha, \beta = 0, \dots, k, \quad (5)$$

where the subscript \mathbf{i} indicates the medium.

By definition, the n^{th} term in \mathbf{U}_i^k is

$$\mathbf{U}_i^k[n] = \lim_{M \rightarrow P, M \in \Omega_i} \frac{\partial^\alpha \mathbf{U}[l]}{\partial x^{\alpha-\beta} \partial y^\beta}, \quad (6)$$

where $\mathbf{U}[l]$ is the l^{th} component of \mathbf{U} . The index n is identified by the function

$$n = \text{idx}(\alpha, \beta, l, d) = \frac{d\alpha(\alpha + 1)}{2} + d\beta + l, \quad l \in 1, \dots, d, \quad (7)$$

where d is the length of \mathbf{U} . The total number of terms in \mathbf{U}_i^k is simply

$$\text{idx}(k, k, d, d) = \frac{dk(k + 1)}{2} + dk + d. \quad (8)$$

As a result, the vectors \mathbf{U}_1^k and \mathbf{U}_2^k contain respectively $3(k^2 + 3k + 2)/2$ and $5(k^2 + 5k + 2)/2$ components.

For the sake of consistency, the following notations are employed for the matrices \mathbf{A} and \mathbf{B} :

$$\mathbf{A}_i = \lim_{M \rightarrow P, M \in \Omega_i} \mathbf{A}, \quad \mathbf{B}_i = \lim_{M \rightarrow P, M \in \Omega_i} \mathbf{B}. \quad (9)$$

B. Arbitrary-order derivatives of the interface constraints

The interface constraints (4) are rewritten as

$$\begin{cases} \mathbf{C}_1^0 \mathbf{U}_1^0 = \mathbf{C}_2^0 \mathbf{U}_2^0 \\ \mathbf{L}_2^0 \mathbf{U}_2^0 = \mathbf{0} \end{cases}, \quad (10)$$

where the matrices $\mathbf{C}_1^0, \mathbf{C}_2^0$ and \mathbf{L}_2^0 are defined by the following expressions:

$$\begin{aligned} \mathbf{C}_1^0 &= \begin{bmatrix} -\frac{dy}{d\tau} & \frac{dx}{d\tau} & & 0 \\ 0 & 0 & -\left(\frac{dx}{d\tau}\right)^2 & -\left(\frac{dy}{d\tau}\right)^2 \end{bmatrix} \\ \mathbf{C}_2^0 &= \begin{bmatrix} -\frac{dy}{d\tau} & \frac{dx}{d\tau} & 0 & 0 & 0 \\ 0 & 0 & \left(\frac{dy}{d\tau}\right)^2 & -2\frac{dx}{d\tau}\frac{dy}{d\tau} & \left(\frac{dy}{d\tau}\right)^2 \end{bmatrix} \\ \mathbf{L}_2^0 &= \begin{bmatrix} 0 & 0 & \frac{dx}{d\tau}\frac{dy}{d\tau} & \left(\left(\frac{dy}{d\tau}\right)^2 - \left(\frac{dx}{d\tau}\right)^2\right) & -\frac{dx}{d\tau}\frac{dy}{d\tau} \end{bmatrix} \end{aligned} \quad (11)$$

Arbitrary-order interface conditions are developed by deriving Eqs. (10) with respect to the variables τ and t . The term $\partial^k \mathbf{T}_i^0 \mathbf{U}_i^0 / \partial \tau^{k-q} \partial t^q$, with \mathbf{T}_i^0 equal to either \mathbf{C}_1^0 , \mathbf{C}_2^0 , or \mathbf{L}_2^0 , is given by the formula (for instance, see Hardy³⁴ and references therein):

$$\frac{\partial^k \mathbf{T}_i^0 \mathbf{U}_i^0}{\partial \tau^{k-q} \partial t^q} = \sum_{q_1=0}^{k-q} \sum_{q_2=0}^q \binom{k-q}{q_1} \binom{q}{q_2} \frac{\partial^{q_1+q_2} \mathbf{T}_i^0}{\partial \tau^{q_1} \partial t^{q_2}} \frac{\partial^{k-q_1-q_2} \mathbf{U}_i^0}{\partial \tau^{k-q-q_1} \partial t^{q-q_2}}. \quad (12)$$

Since the matrix \mathbf{T}_i^0 only depends on the parameter τ , the double sum (12) does not vanish only if $q_2 = 0$. Therefore, Eq. (12) is simplified as

$$\frac{\partial^k \mathbf{T}_i^0 \mathbf{U}_i^0}{\partial \tau^{k-q} \partial t^q} = \sum_{l=0}^{k-q} \binom{k-q}{l} \frac{d^l \mathbf{T}_i^0}{d\tau^l} \frac{\partial^{k-l} \mathbf{U}_i^0}{\partial \tau^{k-q-l} \partial t^q}. \quad (13)$$

The derivatives $d^l \mathbf{T}_i^0 / d\tau^l$ are computed through the formulas for the derivatives of products provided by Hardy³⁴. The function $\partial^q \mathbf{U}_i^0 / \partial t^q$ in (13) is calculated through the Lax-Wendroff (or Cauchy-Kovalevskaya) procedure²⁹, which consists in replacing, in Eqs. (3), the q^{th} -order temporal derivative with spatial derivatives:

$$\frac{\partial^q \mathbf{U}_i^0}{\partial t^q} = (-1)^q \left(\mathbf{A}_i \frac{\partial}{\partial x} + \mathbf{B}_i \frac{\partial}{\partial y} \right)^q \mathbf{U}_i^0. \quad (14)$$

By employing combinatorial rules for the binomial term, the above system is further developed as

$$\frac{\partial^q \mathbf{U}_i^0}{\partial t^q} = \sum_{m=0}^q (-1)^q \mathbf{M}_{i,m,q} \frac{\partial^q \mathbf{U}_i^0}{\partial x^{q-m} \partial y^m}, \quad (15)$$

where $\mathbf{M}_{i,m,q}$ is the sum of the n_{up} unique permutations of $(q-m)$ matrices \mathbf{A}_i and m matrices \mathbf{B}_i .

As an example, $\mathbf{M}_{i,1,3}$ is equal to the sum of the unique permutations of 2 matrices \mathbf{A}_i and 1 matrix \mathbf{B}_i , *i.e.* $\mathbf{A}_i \mathbf{A}_i \mathbf{B}_i$, $\mathbf{A}_i \mathbf{B}_i \mathbf{A}_i$, and $\mathbf{B}_i \mathbf{A}_i \mathbf{A}_i$, *i.e.* $\mathbf{M}_{i,1,3} = \mathbf{A}_i \mathbf{A}_i \mathbf{B}_i + \mathbf{A}_i \mathbf{B}_i \mathbf{A}_i + \mathbf{B}_i \mathbf{A}_i \mathbf{A}_i$. Inserting Eq. (15) in Eq. (13) yields the following expression:

$$\frac{\partial^k \mathbf{T}_i^0 \mathbf{U}_i^0}{\partial \tau^{k-q} \partial t^q} = \sum_{l=0}^{k-q} \sum_{m=0}^q (-1)^q \binom{k-q}{l} \frac{d^l \mathbf{T}_i^0}{d\tau^l} \mathbf{M}_{i,m,q} \frac{\partial^q}{\partial x^{q-m} \partial y^m} \left(\frac{\partial^{k-q-l} \mathbf{U}_i^0}{\partial \tau^{k-q-l}} \right). \quad (16)$$

To calculate the term $\partial^{k-q-l} \mathbf{U} / \partial \tau^{k-q-l}$, a short digression is needed. Suppose that $f, g : \mathbb{R} \mapsto \mathbb{R}$ are functions admitting \mathbf{n} derivatives. According to Mennucci³⁵, the N^{th} -derivative of the composition $f(g(\tau))$ is given by the Faà di Bruno's formula³⁶:

$$\frac{d^N f(g(\tau))}{d\tau^N} = \sum_{n=1}^N \frac{1}{n!} \frac{d^n f(g)}{dg^n} \sum_{(s_1, \dots, s_n) \in \mathcal{C}_N} \binom{N}{s_1, s_2, \dots, s_n} \prod_{r=1}^n \frac{d^{s_r} g(\tau)}{d\tau^{s_r}}. \quad (17)$$

In Eq. (17), the internal sum is over all the compositions \mathcal{C}_N of the integer N into n parts, *i.e.* over all the n -tuples of positive indices s_r , $r = 1, \dots, n$, that satisfy the constraint $s_1 + \dots + s_n = N$. For given n and N , the total number of possible compositions is

$$\sum_{n=1}^N \binom{N-1}{n-1} = 2^{N-1}. \quad (18)$$

By moving the derivative $d^n f(g) / dg^n$ inside the product sign, Expression (17) is rewritten as

$$\frac{d^N f(g(\tau))}{d\tau^N} = \sum_{n=1}^N \frac{1}{n!} \sum_{(s_1, \dots, s_n) \in \mathcal{C}_N} \binom{N}{s_1, s_2, \dots, s_n} \prod_{r=1}^n \left(\frac{d^{s_r} g(\tau)}{d\tau^{s_r}} \frac{d}{dg} \right) f. \quad (19)$$

According to Mishkov³⁷, when a composite function $f(\mathbf{g}(\tau))$ depends on a vector variable \mathbf{g} , $\mathbf{g}(\tau) = [g_1(\tau), g_2(\tau), \dots]$, the derivative $d^{sr}g(\tau)/d\tau^{sr}d/dg$ must be replaced by the operator $(d^{sr}\mathbf{g}/d\tau^{sr} \cdot \nabla)$. As a consequence, the function $\partial^{k-q-l}\mathbf{U}_i/\partial\tau^{k-q-l}$ is equal to

$$\frac{\partial^{k-q-l}\mathbf{U}_i^0}{\partial\tau^{k-q-l}} = \sum_{n=1}^{k-q-l} \frac{1}{n!} \sum_{(s_1, \dots, s_n) \in \mathcal{C}_{k-q-l}} \binom{k-q-l}{s_1, s_2, \dots, s_n} \prod_{r=1}^n \left(\frac{d^{sr}x}{d\tau^{sr}} \frac{\partial}{\partial x} + \frac{d^{sr}y}{d\tau^{sr}} \frac{\partial}{\partial y} \right) \mathbf{U}_i^0. \quad (20)$$

The derivative $\partial^k \mathbf{T}_i^0 \mathbf{U}_i^0 / \partial\tau^{k-q} \partial t^q$ is then given by the formula

$$\begin{aligned} \frac{\partial^k \mathbf{T}_i^0 \mathbf{U}_i^0}{\partial\tau^{k-q} \partial t^q} &= \sum_{l=0}^{k-q} \sum_{m=0}^q \sum_{n=1}^{k-q-l} \sum_{(s_1, \dots, s_n) \in \mathcal{C}_{k-q-l}} \frac{(-1)^q}{n!} \binom{k-q}{l} \binom{k-q-l}{s_1, \dots, s_n} \times \\ &\times \frac{d^l \mathbf{T}_i^0}{d\tau^l} \mathbf{M}_{i,m,q} \frac{\partial^q}{\partial x^{q-m} \partial y^m} \left[\prod_{r=1}^n \left(\frac{d^{sr}x}{d\tau^{sr}} \frac{\partial}{\partial x} + \frac{d^{sr}y}{d\tau^{sr}} \frac{\partial}{\partial y} \right) \right] \mathbf{U}_i^0. \end{aligned} \quad (21)$$

In Eq. (21), the factor between brackets is the product of n binomials of the form $(a_r + b_r)$, with $r = 1, \dots, n$. By virtue of the rule of product, this factor is rewritten as the sum of 2^n terms, each of which is the product of n monomials chosen in the n distinct aforesaid binomials.

Despite its apparent complexity, Eq. (21) is recast in the form

$$\mathbf{T}_i^{q,k} \mathbf{U}_i^k = \frac{\partial^k \mathbf{T}_i^0 \mathbf{U}_i^0}{\partial\tau^{k-q} \partial t^q}. \quad (22)$$

Combining all the derivatives up to the order k yields the expression:

$$\left[\mathbf{T}_i^0 \mathbf{U}_i^0 \quad \frac{\partial \mathbf{T}_i^0 \mathbf{U}_i^0}{\partial\tau} \quad \frac{\partial \mathbf{T}_i^0 \mathbf{U}_i^0}{\partial t} \quad \dots \quad \frac{\partial^k \mathbf{T}_i^0 \mathbf{U}_i^0}{\partial t^k} \right]^T = \left[\mathbf{T}_i^{0,0} \quad \mathbf{T}_i^{0,1} \quad \mathbf{T}_i^{1,1} \quad \dots \quad \mathbf{T}_i^{k,k} \right]^T \mathbf{U}_i^k = \mathbf{T}_i^k \mathbf{U}_i^k. \quad (23)$$

Enforcing the continuity of the derivatives of $\mathbf{C}_i^0 \mathbf{U}_i^0$ and requiring that the derivatives of $\mathbf{L}_2^0 \mathbf{U}_2^0$ vanish on Γ finally leads to the following system:

$$\mathbf{C}_1^k \mathbf{U}_1^k = \mathbf{C}_2^k \mathbf{U}_2^k; \quad (24a)$$

$$\mathbf{L}_2^k \mathbf{U}_2^k = \mathbf{0}. \quad (24b)$$

For a given value of k , there are $(k+1)$ possible mixed derivatives. Consequently, the matrices \mathbf{C}_i^k and \mathbf{L}_i^k have respectively $(k^2 + 3k + 2)/2 \times 2$ and $(k^2 + 3k + 2)/2 \times 1$ rows, and

$$\begin{aligned} \mathbf{C}_i^k &\in \mathbb{R}^{(k^2+3k+2) \times \text{idx}(k,k,d,d)}, \\ \mathbf{L}_i^k &\in \mathbb{R}^{(k^2+3k+2)/2 \times \text{idx}(k,k,d,d)}. \end{aligned}$$

C. Irrotationality of the fluid flow and compatibility conditions for the elastic stresses

As highlighted by Lombard and Piraux¹⁴, the components of \mathbf{U} are not independent, but linked by compatibility relationships. Such constraints, along with their higher-order derivatives, are employed as supplementary constraints for the treatment of the interfaces. For the sake of completeness, they are briefly recalled in the forthcoming lines.

Under the assumptions made in Section II, the fluid flow is irrotational. Therefore, the curl of the acoustic velocity vector must be identically nil:

$$\frac{\partial u_x^f}{\partial y} - \frac{\partial u_y^f}{\partial x} = 0. \quad (25)$$

Deriving Expression (25) $(k - q - 1)$ times with respect to x and q times with respect to y yields the following equation:

$$\frac{\partial^k u_x^f}{\partial x^{k-q-1} \partial y^{q+1}} - \frac{\partial^k u_y^f}{\partial x^{k-q} \partial y^q} = 0, \quad k \geq 1, \quad 0 \leq q \leq (k - 1). \quad (26)$$

For a given order k , $(k^2 + k)/2$ constraints are derived. Moreover, they must be verified at each location (x, y) in the fluid and in particular at the interface point P . Consequently, the vector \mathbf{U}_1^k must satisfy a linear system of the form

$$\mathbf{F}_1^k \mathbf{U}_1^k = \mathbf{0}. \quad (27)$$

The matrix $\mathbf{F}_1^k \in \mathbb{R}^{(k^2+k)/2 \times \text{idx}(k,k,3,3)}$ is computed through the algorithm provided in Algorithm 1.

In a two-dimensional isotropic elastic solid, the three components of the stress tensor are completely determined by the two displacements along the horizontal and vertical axes. Hence, the functions σ_{xx} , σ_{xy} and σ_{yy} are not independent and must verify a compatibility condition. More specifically,

$$\alpha_2 \frac{\partial^2 \sigma_{xx}}{\partial x^2} + \alpha_1 \frac{\partial^2 \sigma_{yy}}{\partial x^2} - \frac{\partial^2 \sigma_{xy}}{\partial x \partial y} + \alpha_1 \frac{\partial^2 \sigma_{xx}}{\partial y^2} + \alpha_2 \frac{\partial^2 \sigma_{yy}}{\partial y^2} = 0. \quad (28)$$

The coefficients α_1 and α_2 are given in terms of the Lamé parameters, i.e. $\alpha_1 = (\bar{\lambda} + 2\bar{\mu})/[4(\bar{\lambda} + \bar{\mu})]$ and $\alpha_2 = -\bar{\lambda}/[4(\bar{\lambda} + \bar{\mu})]$. Deriving Expression (28) $(k - q - 2)$ times with respect to x and q times with respect to y yields the equation

$$\begin{aligned} & \alpha_2 \frac{\partial^k \sigma_{xx}}{\partial x^{k-q} \partial y^q} + \alpha_1 \frac{\partial^k \sigma_{yy}}{\partial x^{k-q} \partial y^q} - \frac{\partial^k \sigma_{xy}}{\partial x^{k-q-1} \partial y^{q+1}} + \alpha_1 \frac{\partial^k \sigma_{xx}}{\partial x^{k-q-2} \partial y^{q+2}} + \\ & \alpha_2 \frac{\partial^k \sigma_{yy}}{\partial x^{k-q-2} \partial y^{q+1}} = 0, \quad k \geq 2, \quad 0 \leq q \leq (k - 2). \end{aligned} \quad (29)$$

For a given order k , $(k^2 - k)/2$ constraints can then be derived. As in the case of the fluid domain, they must be verified at each location (x, y) in the solid and in particular at the interface point P . As a consequence, the vector \mathbf{U}_2^k must satisfy a linear system of the form

$$\mathbf{F}_2^k \mathbf{U}_2^k = \mathbf{0}. \quad (30)$$

The matrix $\mathbf{F}_2^k \in \mathbb{R}^{(k^2-k)/2 \times \text{idx}(k,k,5,5)}$ is calculated through the algorithms provided in Algorithm 2.

```

1:  $q = 1$ ;
2: for  $n = 1 : k$  do
3:   for  $i = 0 : (n - 1)$  do
4:      $\mathbf{F}_1^k(q, \text{idx}(n, i + 1, 1, 3)) = +1$ ;
5:      $\mathbf{F}_1^k(q, \text{idx}(n, i + 0, 2, 3)) = -1$ ;
6:      $q = q + 1$ ;
7:   end for
8: end for

```

Algorithm 1: Algorithm for the computation of the matrix \mathbf{F}_1^k .

```

1:  $q = 1$ ;
2: for  $n = 2 : k$  do
3:   for  $i = 0 : (n - 2)$  do
4:      $\mathbf{F}_2^k(q, \text{idx}(n, i + 0, 3, 5)) = +\alpha_2$ ;
5:      $\mathbf{F}_2^k(q, \text{idx}(n, i + 0, 5, 5)) = +\alpha_1$ ;
6:      $\mathbf{F}_2^k(q, \text{idx}(n, i + 1, 4, 5)) = -1$ ;
7:      $\mathbf{F}_2^k(q, \text{idx}(n, i + 2, 3, 5)) = +\alpha_1$ ;
8:      $\mathbf{F}_2^k(q, \text{idx}(n, i + 2, 5, 5)) = +\alpha_2$ ;
9:      $q = q + 1$ ;
10:  end for
11: end for

```

Algorithm 2: Algorithm for the computation of the matrix \mathbf{F}_2^k .

The constraints (27) and (30) are then used to reduce the number of unknowns in \mathbf{U}_1^k and \mathbf{U}_2^k , respectively. Let $\mathbf{U}_{i,K}^k$ and $\mathbf{U}_{i,R}^k$ be the vectors containing the degrees of freedom to Keep and Remove from \mathbf{U}_i^k , respectively. In the fluid vector, the degrees of freedom $\partial^n u_y / \partial x^{n-q} \partial y^q$, for $n = 1, \dots, k$ and $q = 0, \dots, (n - 1)$, are removed. For the solution in the solid medium, the unknowns $\partial^n \sigma_{yy} / \partial x^{n-q} \partial y^q$, for $n = 2, \dots, k$ and $q = 0, \dots, (n - 2)$, are considered dependent variables. As a consequence, the vectors $\mathbf{U}_{1,K}^k$ and $\mathbf{U}_{2,K}^k$ have $(k^2 + 4k + 3)$ and $(2k^2 + 8k + 5)$ components, respectively. The system $\mathbf{F}_i^k \mathbf{U}_i^k = \mathbf{0}$ is conveniently rearranged as

$$\begin{bmatrix} \mathbf{F}_{i,K}^k & \mathbf{F}_{i,R}^k \end{bmatrix} \begin{bmatrix} \mathbf{U}_{i,K}^k \\ \mathbf{U}_{i,R}^k \end{bmatrix} = \mathbf{0}. \quad (31)$$

Therefore, the relation $\mathbf{U}_{i,R}^k = -\mathbf{F}_{i,R}^k{}^{-1} \mathbf{F}_{i,K}^k \mathbf{U}_{i,K}^k$ holds and the vector \mathbf{U}_i^k is conveniently rewritten as

$$\mathbf{U}_i^k = \mathbf{G}_i^k \mathbf{U}_{i,K}^k, \quad (32)$$

where the matrices $\mathbf{G}_1^k \in \mathbb{R}^{\text{idx}(k,k,3,3) \times (k^2+4k+3)}$ and $\mathbf{G}_2^k \in \mathbb{R}^{\text{idx}(k,k,5,5) \times (2k^2+8k+5)}$ are defined by the formulas

$$\mathbf{G}_1^k = \begin{bmatrix} \mathbf{I}_{k^2+4k+3} \\ -\mathbf{F}_{1,R}^k{}^{-1} \mathbf{F}_{1,K}^k \end{bmatrix}, \quad \mathbf{G}_2^k = \begin{bmatrix} \mathbf{I}_{2k^2+8k+5} \\ -\mathbf{F}_{2,R}^k{}^{-1} \mathbf{F}_{2,K}^k \end{bmatrix}, \quad (33)$$

where $\mathbf{I}_q \in \mathbb{R}^{q \times q}$ is the identity matrix of size $q \times q$. Inserting Expression (32) in Eq. (24b) yields

$$\mathbf{L}_i^k \mathbf{G}_i^k \mathbf{U}_{i,K}^k = \mathbf{0}, \quad (34)$$

where the relation (24b) for $i = 1$ is verified by default being a fluid at rest. Therefore, the vector $\mathbf{U}_{i,K}^k$ belongs to the kernel $\mathcal{L}_{\mathbf{L}_i^k \mathbf{G}_i^k}$ of $\mathbf{L}_i^k \mathbf{G}_i^k$. Let $\mathbf{Z}_{\mathbf{L}_i^k \mathbf{G}_i^k}$ be the matrices whose columns are the basis vectors of $\mathcal{L}_{\mathbf{L}_i^k \mathbf{G}_i^k}$. Then, any $\mathbf{U}_{i,K}^k \in \mathcal{L}_{\mathbf{L}_i^k \mathbf{G}_i^k}$ can be expressed as

$$\mathbf{U}_{i,K}^k = \mathbf{Z}_{\mathbf{L}_i^k \mathbf{G}_i^k} \mathbf{V}_{i,K}^k. \quad (35)$$

The vectors \mathbf{V}_1^k and \mathbf{V}_2^k have respectively $(k^2 + 4k + 3)$ and $(3k^2 + 13k + 8)/2$ components, and, consequently, $\mathbf{Z}_{\mathbf{L}_1^k \mathbf{G}_1^k} \in \mathbb{R}^{(k^2+4k+3) \times (k^2+4k+3)}$ and $\mathbf{Z}_{\mathbf{L}_2^k \mathbf{G}_2^k} \in \mathbb{R}^{(2k^2+8k+5) \times (3k^2+13k+8)/2}$. The matrix $\mathbf{Z}_{\mathbf{L}_i^k \mathbf{G}_i^k}$ is deduced from a Singular Value Decomposition (SVD) of $\mathbf{L}_i^k \mathbf{G}_i^k$.

The interface conditions $\mathbf{C}_1^k \mathbf{U}_1^k = \mathbf{C}_2^k \mathbf{U}_2^k$ are finally rewritten as

$$\mathbf{S}_1^k \mathbf{V}_1^k = \mathbf{S}_2^k \mathbf{V}_2^k, \quad (36)$$

where the matrices \mathbf{S}_1^k and \mathbf{S}_2^k are defined by the following formulas:

$$\begin{aligned} \mathbf{S}_1^k &= \mathbf{C}_1^k \mathbf{G}_1^k \mathbf{Z}_{\mathbf{L}_1^k \mathbf{G}_1^k} \in \mathbb{R}^{(k^2+3k+2) \times (k^2+4k+3)}, \\ \mathbf{S}_2^k &= \mathbf{C}_2^k \mathbf{G}_2^k \mathbf{Z}_{\mathbf{L}_2^k \mathbf{G}_2^k} \in \mathbb{R}^{(k^2+3k+2) \times (3k^2+13k+8)/2}. \end{aligned} \quad (37)$$

To employ the ESIM, the solution \mathbf{V}_2^k must be expressed as a function of \mathbf{V}_1^k , and viceversa. System (36) is underdetermined and is solved through the SVD method. Its general solution is

$$\mathbf{V}_2^k = \mathbf{S}_2^{k+} \mathbf{S}_1^k \mathbf{V}_1^k + \left[\mathbf{I}_{(3k^2+13k+8)/2} - \mathbf{S}_2^{k+} \mathbf{S}_2^k \right] \mathbf{\Lambda}_1^k, \quad (38)$$

where \mathbf{S}_2^{k+} is the pseudoinverse of \mathbf{S}_2^k and $\mathbf{\Lambda}_1^k \in \mathbb{R}^{(3k^2+13k+8)/2 \times 1}$ is any real column vector.

An analogous result holds for \mathbf{V}_1^k ,

$$\mathbf{V}_1^k = \mathbf{S}_1^{k+} \mathbf{S}_2^k \mathbf{V}_2^k + \left[\mathbf{I}_{(k^2+4k+3)} - \mathbf{S}_1^{k+} \mathbf{S}_1^k \right] \mathbf{\Lambda}_2^k, \quad (39)$$

where $\mathbf{S}_1^{k+} \in \mathbb{R}^{(k^2+4k+3) \times (k^2+3k+2)}$ is the pseudoinverse of \mathbf{S}_1^k and $\mathbf{\Lambda}_2^k \in \mathbb{R}^{(k^2+4k+3) \times 1}$ is any real column vector.

IV. ADESIM $s - k$ METHOD

In this section, the ADESIM $s - k$ method is presented. The ADER scheme employed for solving the governing system (3) is first outlined. The ESIM procedure, with the novel algorithm for computing arbitrary-order spatial derivatives of the interface conditions outlined in Section III C, is then recalled for the sake of completeness.

A. ADER schemes for the governing system (3)

Define a time step Δt and a uniform Cartesian grid, consisting of N_x and N_y nodes along the x - and y -axes, respectively (cf. Figure 2). The spacings are labeled as Δx and Δy and, for the sake of simplicity, they are assumed equal throughout this paper, $\Delta x = \Delta y$. The interface Γ is immersed in the computational mesh. Consider a generic point M of coordinates $x_i = i\Delta x$ and $y_j = j\Delta y$, with $i = 1, \dots, N_x$ and $j = 1, \dots, N_y$, and suppose temporarily that M is sufficiently far from Γ (blue node in Figure 2). The function $\mathbf{U}(x, y, t)$ is therefore smooth in a neighborhood of M . The term $\mathbf{U}(x_i, y_j, t_{n+1})$, evaluated at the instant $t_{n+1} = (n + 1)\Delta t$, can be formally computed through a Taylor series around t_n :

$$\mathbf{U}(x_i, y_j, t_{n+1}) = \mathbf{U}(x_i, y_j, t_n) + \sum_{q=1}^{\infty} \frac{\Delta t^q}{q!} \left. \frac{\partial^q \mathbf{U}}{\partial t^q} \right|_{x=x_i, y=y_j, t=t_n}. \quad (40)$$

Using Eq. (3) to replace the temporal derivative by spatial derivatives and employing the combinatorial rules for the binomial term, as done in Eq. (15), yields the expression

$$\begin{aligned} \mathbf{U}(x_i, y_j, t_{n+1}) &= \mathbf{U}(x_i, y_j, t_n) + \\ &\sum_{q=1}^s \sum_{m=0}^q \frac{(-1)^q \Delta t^q}{q!} \mathbf{M}_{m,q} \left. \frac{\partial^q \mathbf{U}}{\partial x^{q-m} \partial y^m} \right|_{x=x_i, y=y_j, t=t_n} + \mathcal{O}(\Delta t^{s+1}). \end{aligned} \quad (41)$$

Note that the temporal Taylor series has been truncated at the order s , with only even s considered in this work. The matrix $\mathbf{M}_{m,q}$ is defined as in Section III. A numerical scheme is then obtained by replacing the spatial derivatives with finite-difference formulas. To this end, a square stencil centered at the point (x_i, y_j) and employing at most $(s + 1) \times (s + 1)$ nodes is used. The approximation $\mathbf{U}_{i,j}^{n+1}$ of the solution $\mathbf{U}(x_i, y_j, t_{n+1})$ is written as

$$\mathbf{U}_{i,j}^{n+1} = \mathbf{U}_{i,j}^n + \sum_{\alpha=-s/2}^{s/2} \sum_{\beta=-s/2}^{s/2} \mathbf{D}_{\alpha,\beta} \mathbf{U}_{i+\alpha, j+\beta}^n. \quad (42)$$

The numerical scheme (42) has the structure of a single-step finite difference method, with a stencil of $(s + 1) \times (s + 1)$ nodes centered around the point M , and can be abstractly rewritten as

$$\mathbf{U}_{i,j}^{n+1} = \mathcal{H} \left(\mathbf{U}_{i-s/2, j-s/2}^n, \dots, \mathbf{U}_{i+s/2, j+s/2}^n \right), \quad (43)$$

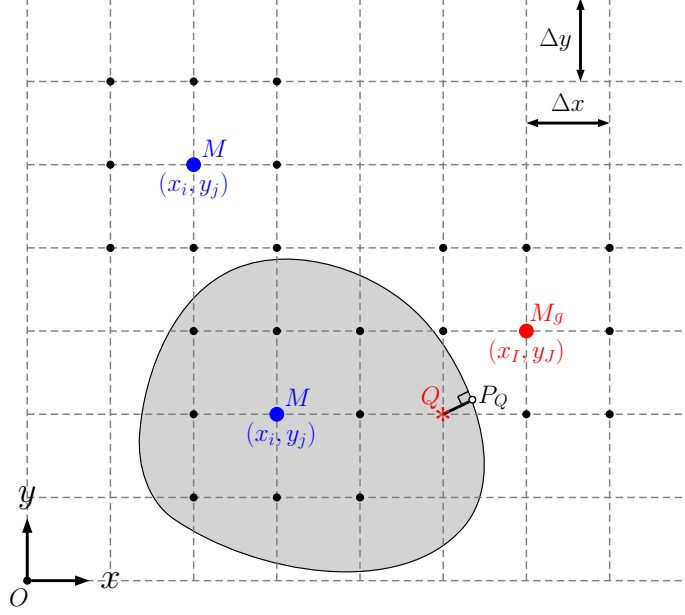


FIG. 2. (color online) Computational grid

where \mathcal{H} is a linear discrete operator. The scheme \mathcal{H} is of order s in space and in time, *i.e.* the local truncation error behaves as $\mathcal{O}(\Delta t^{s+1}, \Delta x^{s+1}, \Delta y^{s+1})$. Moreover, the grid spacing Δx is related to the time step Δt by the Courant-Friedrichs-Lewy number

$$\text{CFL} = \max(\bar{c}_t, \bar{c}_p, \bar{c}_s) \frac{\Delta t}{\Delta x}, \quad (44)$$

whose maximum value is $1/\sqrt{2}$ for $s = 2$ and $\gtrsim 1$ for $s \geq 4$ ³⁰.

B. Explicit simplified interface method (ESIM)

Consider at present a node M_g of coordinates (x_I, y_J) and close to the interface Γ (cf. Figure 2). Assume that one of the stencil points Q of coordinates $(x_{I+\alpha^*}, y_{J+\beta^*})$, $\alpha^*, \beta^* \in [-s/2, s/2]$, $\alpha^* \neq 0, \beta^* \neq 0$, lies in the adjacent domain (red asterisk in Figure 2). The node M_g is therefore regarded as irregular and Formula (43) cannot be applied, without modifications, to calculate the approximation $\mathbf{U}_{I,J}^{n+1}$ of $\mathbf{U}(x_I, y_J, t_{n+1})$. The ESIM method provides a strategy to overcome this issue. Its basic idea is to employ Expression (43) at the node M_g as well, upon replacing the term $\mathbf{U}_{I+\alpha^*, J+\beta^*}^n$ with an appropriate modified or ghost value $\mathbf{U}_{I+\alpha^*, J+\beta^*}^{n*}$. As an illustration, the numerical solution $\mathbf{U}_{I,J}^{n+1}$ at the red node displayed in Figure 2 would be computed as

$$\begin{aligned} \mathbf{U}_{I,J}^{n+1} = \mathcal{H} & \left(\mathbf{U}_{I-1,J-1}^{n*}, \mathbf{U}_{I+0,J-1}^n, \mathbf{U}_{I+1,J-1}^n, \right. \\ & \mathbf{U}_{I-1,J+0}^n, \mathbf{U}_{I+0,J+0}^n, \mathbf{U}_{I+1,J+0}^n, \\ & \left. \mathbf{U}_{I-1,J+1}^n, \mathbf{U}_{I+0,J+1}^n, \mathbf{U}_{I+1,J+1}^n \right). \end{aligned} \quad (45)$$

Let Ω_i and $\underline{\Omega}_i$ be the domain of the irregular node M_g and the opposite medium, respectively. Moreover, let P_Q be the orthogonal projection of Q on the interface Γ , with coordinates (x_{P_Q}, y_{P_Q}) . The ghost value $\mathbf{U}_{I+\alpha^*, J+\beta^*}^{n^*}$ can be interpreted as the point value of a smooth extension \mathbf{U}^* of the mechanical field \mathbf{U} in Ω_i into the domain $\underline{\Omega}_i$ (the fluid solution is smoothly extended in the solid side and viceversa). Such an extension is defined by a k^{th} -order Taylor series around the point P_Q seen from the domain Ω_i :

$$\mathbf{U}^*(x, y, t) = \mathbf{\Pi}_i^k(x, y) \mathbf{U}_i^k(x_{P_Q}, y_{P_Q}, t). \quad (46)$$

In Eq. (46), the components of the matrix $\mathbf{\Pi}_i^k \in \mathbb{R}^{d \times \text{idx}(k, k, d, d)}$ are given by the expression

$$\mathbf{\Pi}_i^k[l, \text{idx}(v, w, l, d)](x, y) = \frac{(x - x_{P_Q})^{v-w} (y - y_{P_Q})^w}{(v-w)! w!}, \quad l = 1, \dots, d, \quad r, s = 1, \dots, k. \quad (47)$$

The modified value $\mathbf{U}_{I+\alpha^*, J+\beta^*}^{n^*}$ is then calculated as

$$\mathbf{U}_{I+\alpha^*, J+\beta^*}^{n^*} = \mathbf{\Pi}_i^k(x_{I+\alpha^*}, y_{J+\beta^*}) \mathbf{U}_{i, P_Q}^{k, n}, \quad (48)$$

where $\mathbf{U}_{i, P_Q}^{k, n}$ is an approximation of the vector $\mathbf{U}_i^k(x_{P_Q}, y_{P_Q}, t_n)$. Therefore, computing $\mathbf{U}_{I+\alpha^*, J+\beta^*}^{n^*}$ is tantamount to estimate $\mathbf{U}_{i, P_Q}^{k, n}$.

Assume at present that the point Q is located in the solid side, as in Figure 2. In order to evaluate $\mathbf{U}_{i, P_Q}^{k, n}$, a set \mathcal{B} of grid nodes surrounding P_Q is employed (cf. Figure 3). This

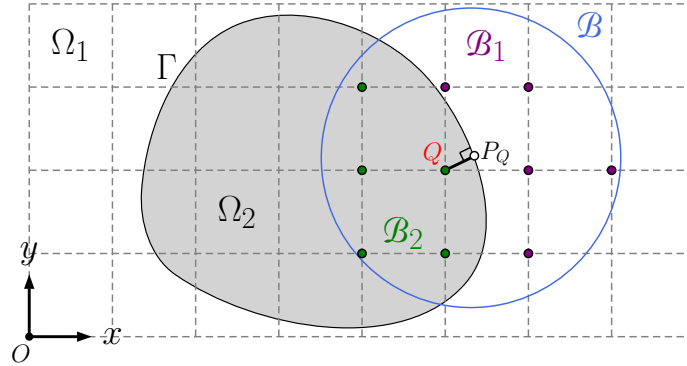


FIG. 3. (color online) Set of nodes \mathcal{B} for the estimation of the vector $\mathbf{U}_{i, P_Q}^{k, n}$

set is enclosed in a circle centered at the point P_Q with a radius $r_{\mathcal{B}}$ and is divided into two subsets \mathcal{B}_i , $i = 1, 2$, by the interface Γ . The solution at a node of indexes (i, j) in the subset \mathcal{B}_1 is given, at the instant t_n , by the expression

$$\begin{aligned} \mathbf{U}(x_i, y_j, t_n) &= \mathbf{\Pi}_1^k(x_i, y_j) \mathbf{U}_1^k(t_n) + \mathcal{O}(\Delta x^{k+1}) \\ &= \mathbf{\Pi}_1^k(x_i, y_j) \mathbf{G}_1^k \mathbf{Z}_{\mathbf{L}_1^k \mathbf{G}_1^k} \mathbf{V}_1^k(t_n) + \mathcal{O}(\Delta x^{k+1}), \end{aligned} \quad (49)$$

which is rewritten as

$$\mathbf{U}(x_i, y_j, t_n) = \mathbf{\Pi}_1^k(x_i, y_j) \mathbf{G}_1^k \mathbf{Z}_{\mathbf{L}_1^k \mathbf{G}_1^k} \begin{bmatrix} \mathbf{I}_{(k^2+4k+3)} & \mathbf{O}_{\Lambda_1^k} \end{bmatrix} \begin{bmatrix} \mathbf{V}_1^k(t_n) \\ \Lambda_1^k(t_n) \end{bmatrix} + \mathcal{O}(\Delta x^{k+1}), \quad (50)$$

where $\mathbf{O}_{\Lambda_1^k}$ is the null matrix of size $(k^2 + 4k + 3) \times (3k^2 + 13k + 8)/2$. At a point of indexes (i, j) located in the subset \mathcal{B}_2 , the solution at the instant t_n is instead given by the following formula:

$$\begin{aligned} \mathbf{U}(x_i, y_j, t_n) &= \mathbf{\Pi}_2^k(x_i, y_j) \mathbf{U}_2^k(t_n) + \mathbf{O}(\Delta x^{k+1}) \\ &= \mathbf{\Pi}_2^k(x_i, y_j) \mathbf{G}_2^k \mathbf{Z}_{\mathbf{L}_2^k \mathbf{G}_2^k} \mathbf{V}_2^k(t_n) + \mathbf{O}(\Delta x^{k+1}). \end{aligned} \quad (51)$$

Using Eq. (38) to recast the vector \mathbf{V}_2^k as a function of the vector \mathbf{V}_1^k yields

$$\mathbf{U}(x_i, y_j, t_n) = \mathbf{\Pi}_2^k(x_i, y_j) \mathbf{G}_2^k \mathbf{Z}_{\mathbf{L}_2^k \mathbf{G}_2^k} \begin{bmatrix} \mathbf{S}_2^{k+} \mathbf{S}_1^k & (\mathbf{I}_{(3k^2+13k+8)/2} - \mathbf{S}_2^{k+} \mathbf{S}_2^k) \end{bmatrix} \begin{bmatrix} \mathbf{V}_1^k(t_n) \\ \mathbf{\Lambda}_1^k(t_n) \end{bmatrix} + \mathbf{O}(\Delta x^{k+1}). \quad (52)$$

Combining Equation (50) and Equation (52) for all the nodes in \mathcal{B} leads to an expression of the following form:

$$(\mathcal{U}^n)_{\mathcal{B}} \equiv \begin{bmatrix} \mathbf{U}(x_{i_1}, y_{j_1}, t_n) \\ \mathbf{U}(x_{i_2}, y_{j_2}, t_n) \\ \vdots \end{bmatrix} = \mathbf{M}_{\mathcal{B},1}(x_{i_1}, y_{j_1}, x_{i_2}, y_{j_2}, \dots) \begin{bmatrix} \mathbf{V}_1^k(t_n) \\ \mathbf{\Lambda}_1^k(t_n) \end{bmatrix} + \begin{bmatrix} \mathbf{O}(\Delta x^{k+1}) \\ \vdots \\ \mathbf{O}(\Delta x^{k+1}) \end{bmatrix}. \quad (53)$$

The radius $r_{\mathcal{B}}$ of \mathcal{B} is chosen in such a way that System (53) is overdetermined. A convenient restriction $\overline{\mathbf{M}}_{\mathcal{B},1}^+$ of the pseudoinverse $\mathbf{M}_{\mathcal{B},1}$ of the matrix $\mathbf{M}_{\mathcal{B},1}$ provides an approximation of the unknown vector \mathbf{V}_1^k and

$$\mathbf{U}_{i,P_Q}^{k,n} = \mathbf{G}_1^k \mathbf{Z}_{\mathbf{L}_1^k \mathbf{G}_1^k} \overline{\mathbf{M}}_{\mathcal{B},1}^+ (\mathcal{U}^n)_{\mathcal{B}}. \quad (54)$$

The modified value $\mathbf{U}_{I+\alpha^*, J+\beta^*}^{n*}$ is finally calculated as

$$\mathbf{U}_{I+\alpha^*, J+\beta^*}^{n*} = \mathbf{\Pi}_i^k(x_{I+\alpha^*}, y_{J+\beta^*}) \mathbf{G}_1^k \mathbf{Z}_{\mathbf{L}_1^k \mathbf{G}_1^k} \overline{\mathbf{M}}_{\mathcal{B},1}^+ (\mathcal{U}^n)_{\mathcal{B}}. \quad (55)$$

For a node Q in the fluid side, an analogous procedure leads to a formula of the form

$$\mathbf{U}_{I+\alpha^*, J+\beta^*}^{n*} = \mathbf{\Pi}_i^k(x_{I+\alpha^*}, y_{J+\beta^*}) \mathbf{G}_2^k \mathbf{Z}_{\mathbf{L}_2^k \mathbf{G}_2^k} \overline{\mathbf{M}}_{\mathcal{B},2}^+ (\mathcal{U}^n)_{\mathcal{B}}. \quad (56)$$

The computations of $\mathbf{U}_{i,P_Q}^{k,n}$ and $\mathbf{U}_{I+\alpha^*, J+\beta^*}^{n*}$ involve the high-order constraints described in Section III. As a result, the modified or ghost value $\mathbf{U}_{I+\alpha^*, J+\beta^*}^{n*}$ implicitly allows taking into account the interface conditions, which are necessary for a correct description of the reflection and transmission phenomena of waves at a boundary between different media. The above procedure must be repeated at each time step for all irregular nodes and grid points located in the opposite side of Γ , before using the ghost values in the scheme (43).

V. NUMERICAL EXPERIMENTS

Two numerical experiments are carried out. In the first test case, the propagation of a plane wave through a flat fluid/solid interface is simulated. This benchmark aims at

demonstrating the improvement of the accuracy and of the convergence rate when increasing the orders s and k of the ADER scheme and the interface treatment. The second experiment concerns the acoustic scattering of a cylindrical pulse by a water-filled aluminum cylindrical shell immersed in water. Its goals are to show the ability of the ADESIM $s - k$ method to handle curved interfaces and to examine the resolutions in terms of points-per-wavelength for various values of s and k .

A. First test case

In the first test case, the material boundary is described by a parameter τ as

$$\Gamma = \{(x, y) \in \mathbb{R}^2 \mid x(\tau) = 0, y(\tau) = \tau, \tau \in \mathbb{R}\}, \quad (57)$$

and the physical properties of the media are set to $\bar{\rho}_f = 1000 \text{ kg m}^{-3}$, $\bar{c}_f = 1500 \text{ m s}^{-1}$, $\bar{\rho}_s = 2600 \text{ kg m}^{-3}$, $\bar{c}_p = 4000 \text{ m s}^{-1}$, and $\bar{c}_s = 2000 \text{ m s}^{-1}$. The initial field is a plane wave propagating in the fluid with an angle ϑ of 21° with respect to the horizontal axis and is defined by the expression

$$\mathbf{U}(x, y, t) = - \left[\frac{\cos(\vartheta)}{\bar{c}_f} \quad \frac{\sin(\vartheta)}{\bar{c}_f} \quad \bar{\rho}_f \right]^T \mathcal{F} \left(t - \frac{x}{c_1} \right), \quad (58)$$

for $t = 0$. The function \mathcal{F} is a C^6 spatially-bounded combination of truncated sinusoids and is given by the formula²¹

$$\mathcal{F}(\xi) = \begin{cases} \sum_{m=1}^4 \mathbf{a}_m \sin(\mathbf{b}_m \omega_0 \xi) & \xi \in \left[0, \frac{2\pi}{\omega_c} \right] \\ 0 & \text{otherwise} \end{cases}, \quad (59)$$

where $\mathbf{a}_1 = 1$, $\mathbf{a}_2 = -21/32$, $\mathbf{a}_3 = 63/768$, $\mathbf{a}_4 = -1/512$, $\mathbf{b}_m = 2^{m-1}$, and $\omega_0 = 2\pi \times 8 \text{ kHz}$.

The physical domain of interest spans the square $[-2, 2] \text{ m} \times [-2, 2] \text{ m}$. At its boundaries, the analytical solution provided by Lombard³² is employed to update the mechanical field \mathbf{U} . Different simulations are performed with various values of Δx , s , and k . The Courant-Friedrichs-Lewy number CFL is set equal to 0.95 for $s \geq 4$ and to 0.95/1.5 for $s = 2$. The numerical results are compared with the analytical solution.

The stresses σ_{yy} obtained at three different instants of time with $\Delta x = 1/256 \text{ m}$, $s = 6$ and $k = 5$ are reported in Figure 4 (in the fluid $\sigma_{yy} = -p$). In the fluid, the mechanical field consists of an incident and of a reflected acoustic waves. In the solid, transmitted P- and S-waves are observed.

The errors in norm \mathcal{L}_∞ calculated at the instant $t = 7.4 \times 10^{-4} \text{ s}$, on the line $y = -0.1 \text{ m}$, are displayed in Figure 5 with the convergence rates. In agreement with the theoretical results of Gustafsson²⁷, a $(s - 1)^{\text{th}}$ -order interface treatment coupled with a s^{th} -order ADER scheme is sufficient to maintain s^{th} -order global accuracy. The schemes ADESIM

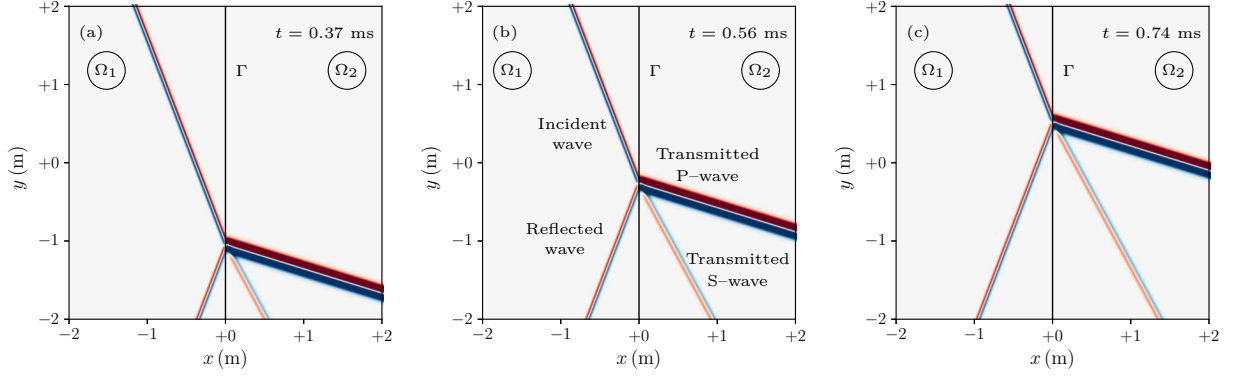


FIG. 4. (color online) First test case. Stress fields σ_{yy} at three different instants of time obtained through the scheme ADESIM 6 – 5.

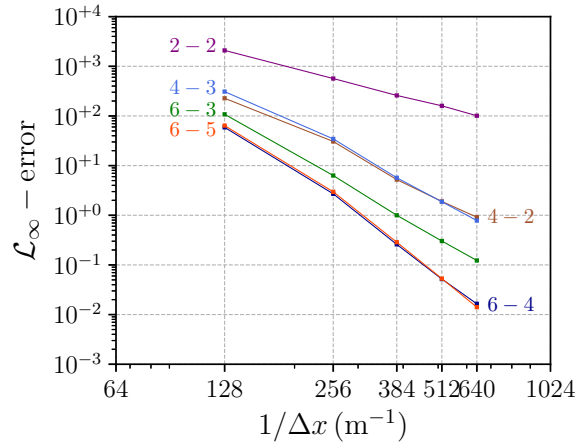


FIG. 5. (color online) First test case. Convergence rates.

2 – 2, ADESIM 4 – 2, ADESIM 4 – 3, ADESIM 6 – 3, ADESIM 6 – 4 and ADESIM 6 – 5 exhibits indeed the following rounded convergence rates: 2, 3, 4, 4, 5, 6.

The results obtained with $\Delta x = 1/128\text{m}$ and through different values of s and k are illustrated in Figures 6. In particular, the signals of pressure calculated at the point of coordinates $(-1, 0)\text{m}$ are plotted in Figure 6(a); the signals of vertical stress σ_{yy} associated with the transmitted P- and S-waves and obtained at the node of coordinates $(0.8, 0)\text{m}$ are displayed in Figures 6(c) and 6(e), respectively. The corresponding one-sided energy spectral densities are shown in Figures 6(b), 6(d) and 6(f). While numerical dispersion is observed on the curves computed with the second-order ADESIM scheme, the signals calculated through the fourth- and sixth-order methods are in good agreement with the exact solutions. Increasing the orders of both the ADER scheme and of the interface treatment

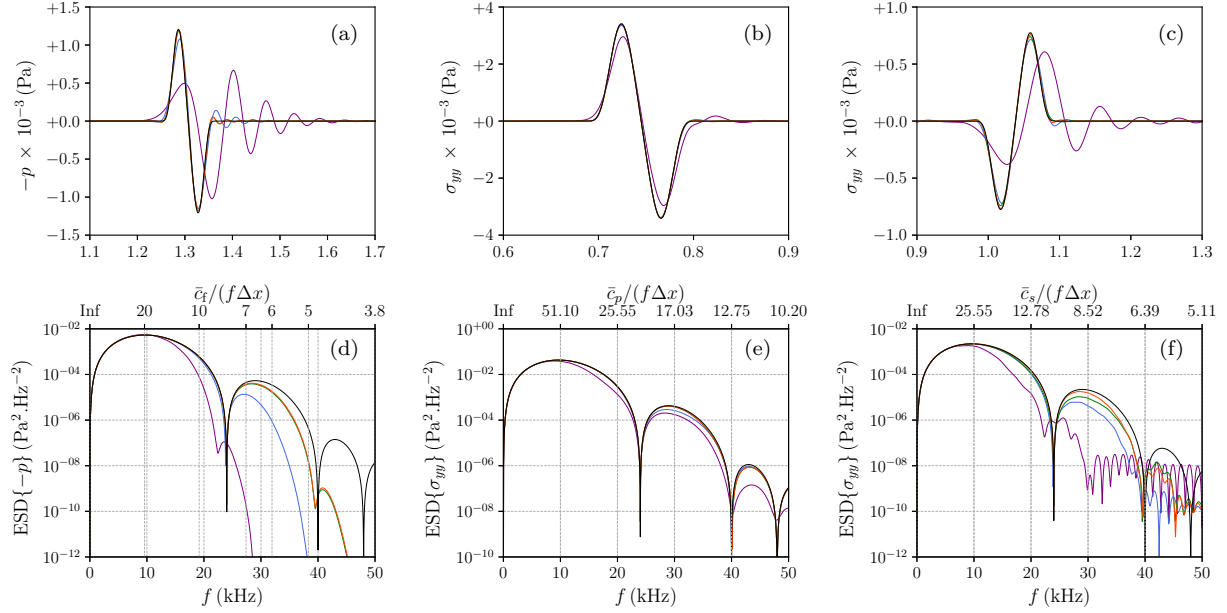


FIG. 6. (color online) First test case. (a) Reflected pressures at the point $(-1, 0)$ m. (b) Transmitted P-waves and (c) transmitted S-waves at the point $(0.8, 0)$ m. (d)-(e)-(f) Corresponding one-sided energy spectral densities. Results obtained analytically (black lines) and numerically, with $\Delta x = 1/128$ m, through the following methods: ADESIM 2 – 2 (purple lines), ADESIM 4 – 3 (blue lines), ADESIM 6 – 3 (green lines), ADESIM 6 – 5 (orange lines).

improves the numerical accuracy.

B. Second test case

In the second test case, the internal and external fluid/solid interfaces are described by the parametric equations

$$\begin{aligned} \Gamma_{\text{internal}} &= \{(x, y) \in \mathbb{R}^2 \mid x(\tau) = r_i \cos(\tau) + 0.5, y(\tau) = r_i \sin(\tau), \tau \in [0, 2\pi[\}, \\ \Gamma_{\text{external}} &= \{(x, y) \in \mathbb{R}^2 \mid x(\tau) = r_e \cos(\tau) + 0.5, y(\tau) = r_e \sin(\tau), \tau \in [0, 2\pi[\}, \end{aligned} \quad (60)$$

where $r_i = 0.4$ m and $r_e = 0.5$ m. The density and the speed of sound of the internal and external fluids are $\bar{\rho}_f = 1000 \text{ kg m}^{-3}$ and $\bar{c}_f = 1500 \text{ m s}^{-1}$. The properties of the solid are $\bar{\rho}_s = 2700 \text{ kg m}^{-3}$, $\bar{c}_p = 6420 \text{ m s}^{-1}$, and $\bar{c}_s = 3040 \text{ m s}^{-1}$. The initial mechanical field is nil and an incident cylindrical pulse (Ricker wavelet) is excited in the external fluid by the pressure source

$$\mathbf{S}(x, y, t) = -\frac{1}{\pi\alpha^2} \left[1 - \frac{\omega_c^2}{2} (t - t_c)^2 \right] e^{-\omega_c^2(t-t_c)^2/4} e^{-(x-x_c)^2/\alpha^2 - (y-y_c)^2/\alpha^2} [0 \ 0 \ 1]^T, \quad (61)$$

where $\omega_c = 2\pi \times 20$ kHz, $t_c = 0.1$ ms, $x_c = -0.5$ m, $y_c = 0$ m, and $\alpha = 0.005$ m. The term (61) is integrated in the numerical solution at the end of each time step through the Euler method.

The computational frame spans the square $[-1, 2] \text{ m} \times [-1.5, 1.5] \text{ m}$. At its boundaries, the radiation conditions proposed by Tam and Webb³⁸ are employed to minimize the reflections of outgoing waves. Simulations are performed with $\Delta x = 3.75 \times 10^{-3}$ m by employing the following schemes: ADESIM 2 – 2, ADESIM 4 – 3, ADESIM 6 – 3, and ADESIM 6 – 5. The Courant-Friedrichs-Lewy number CFL is set equal to 0.95 for $s \geq 4$ and to 0.95/1.5 for $s = 2$. The numerical results are compared with the analytical solution. The latter is computed via standard techniques for acoustic scattering by cylindrical shells³⁹, with the incident acoustic field calculated as suggested in Sabatini et al.⁴⁰.

The stress fields σ_{xx} obtained at four different instants of time through the scheme ADESIM 6 – 5 are displayed in Figure 7. At $t = 0.33$ ms (cf. Figure 7(a)), a cylindrical impulsive wave has been excited in the ambient fluid and is travelling toward the shell. At $t = 0.66$ ms (cf. Figure 7(b)), the pulse has been reflected by the external interface and is propagating through the object. At $t = 1.32$ ms (cf. Figure 7(c)) and $t = 2.74$ ms (cf. Figure 7(d)), the scattered field has filled the whole physical domain of interest.

The signals of pressure calculated at the point of coordinates $(-0.5, 0)$ m are shown in Figures 8(a) and 8(b) along with the analytical solution. The corresponding one-sided energy spectral densities are displayed in Figure 8(c). While numerical dispersion is observed on the results computed with the second- and the fourth-order ADESIM schemes, the curves calculated through the sixth-order methods are in excellent agreement with the exact solution. This trend is also visible in the ESD diagram, which clearly shows the increase of the numerical accuracy with the orders s . As an illustration, for $s = 6$, appreciable differences between the numerical and the exact ESDs only appear for frequencies higher than about 52 kHz. In order to quantify the accuracies of the computations, a relative error $\mathcal{E}_{\text{FT}\{-p\}}$ for the modulus of the Fourier transform of a numerical time series is introduced:

$$\mathcal{E}_{\text{FT}\{-p\}}(f) = \frac{|\text{FT}\{-p_{\text{numerical}}\}(f) - \text{FT}\{-p_{\text{analytical}}\}(f)|}{|\text{FT}\{-p_{\text{analytical}}\}(f)|}. \quad (62)$$

For each numerical signal, the function $\mathcal{E}_{\text{FT}\{-p\}}(f)$ is smoothed through a moving average with a window length of 2 kHz. The resulting curves are plotted in Figure 8(d). For each scheme, the smallest resolved wavelength λ_{\min} is then defined as the minimum value of $\lambda = \bar{c}_f/f$ such that $\mathcal{E}_{\text{FT}\{-p\}}(f) < 10^{-1}$. The results are reported in Table I. Note that with ADESIM 6 – 5, the largest resolved frequency f_{\max} is 342% higher than the one resolved with standard method ADESIM 2 – 2¹⁴. Consequently, the number of points required for resolving the smallest wavelength λ_{\min} drastically reduces by the same percentage amount, bringing to a significant gain in computational memory requirements.

Increasing the orders of both the ADER scheme and the interface treatment, while keeping the grid spacing Δx constant, clearly enhances the numerical resolution. As an illustration,

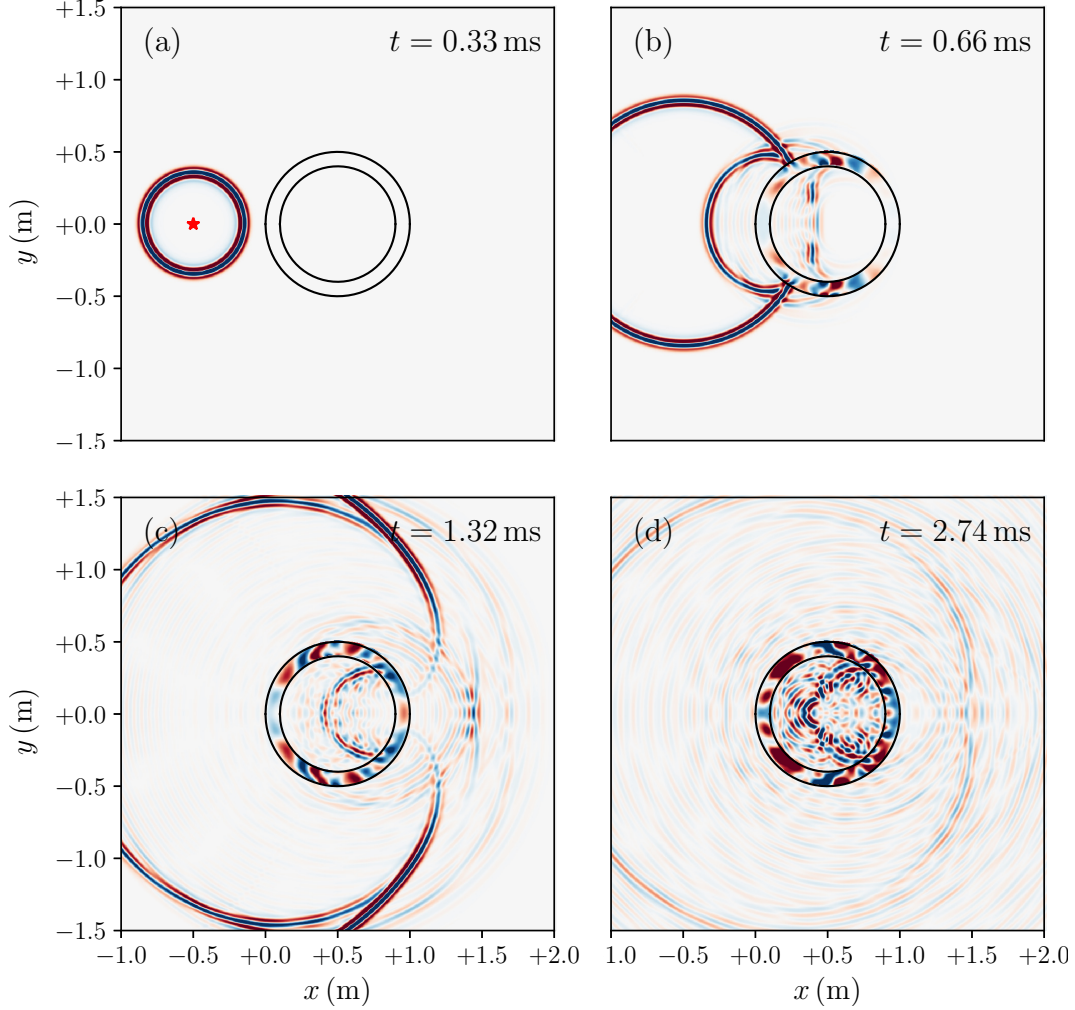


FIG. 7. (color online) Second test case. Stress fields σ_{xx} at four different instants of time obtained through the scheme ADESIM 6 – 5.

Method $s - k$	Max. resolved f (Hz)	$\lambda_{\min}/\Delta x$
ADESIM 2 – 2	15.38	26.01
ADESIM 4 – 3	34.39	11.63
ADESIM 6 – 3	51.75	07.73
ADESIM 6 – 5	52.63	07.60

TABLE I. Second test case. Numerical accuracies in terms of points-per-wavelength.

a sixth-order ADER method coupled with a fifth-order ESIM achieves a resolution of about $\lambda_{\min}/\Delta x = 7.6$ points-per-wavelength, which is comparable to the accuracy of very-high-quality solvers, such as the well-known SPEC-FEM code based on the spectral element method^{8,11–13}. On the other hand, for a fixed value of λ_{\min} , the minimum Δx verifying the resolution requirements grows roughly linearly with s . As a consequence, for a given

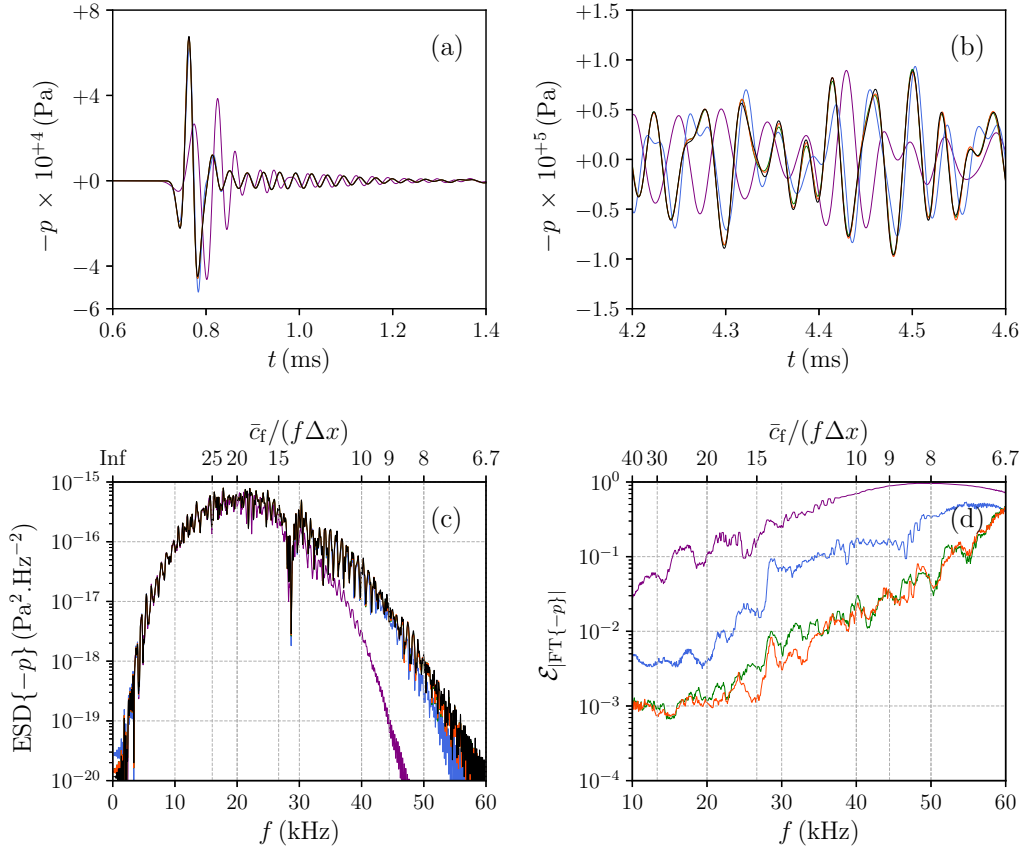


FIG. 8. (color online) Second test case. (a)-(b) Signals at the point of coordinates $(-0.5, 0)$ m obtained analytically (black lines) and through the schemes ADESIM 2–2 (purple lines), ADESIM 4–3 (blue lines), ADESIM 6–3 (green lines), ADESIM 6–5 (orange lines). (c) Corresponding one-sided energy spectral densities. (d) Relative errors for the absolute values of the Fourier transforms of the numerical signals.

value of the maximum frequency to be resolved and for given dimensions of the physical domain of interest, the number of points per direction decreases linearly with s and the total number of nodes diminishes quadratically. This study clearly shows the potential gain in the computational cost offered by the ADESIM $s - k$ method over classically-employed FD schemes.

VI. CONCLUSION

An arbitrary-order immersed interface method has been developed for the simulation of the two-dimensional linear propagation of mechanical waves in heterogeneous media including fluid and solid domains. The proposed technique uses ADER schemes of arbitrary accuracy in space and in time to solve the governing equations and employs the “explicit

simplified interface method” (ESIM) by Lombard and Piraux¹⁴ for the treatment of the interfaces. In order to implement the ESIM, arbitrary-order spatial derivatives of the interface conditions are required. To this end, an algorithm for their numerical computation, which does not require the knowledge of their explicit analytical expressions, has been derived. This procedure could be extremely useful for future developments in three dimensions. Two numerical experiments have been finally examined: the propagation of a plane wave through a flat fluid/solid interface and the propagation of a cylindrical pulse through an aluminum shell immersed in water and filled with water. The improvement of the convergence rate and of the numerical accuracy when increasing both the order of the ADER scheme and of the interface treatment has been more specifically demonstrated. In particular, a sixth-order ADER method coupled with a fifth-order ESIM allows achieving a resolution of about 7.6 points-per-wavelength, which is comparable to the accuracy of very-high-quality solvers, such as the well-known SPECFEM code.

The present study leaves various unanswered questions that will be the subject of future investigations. Firstly, specific strategies must be developed for the treatment of non-smooth and crossing interfaces. Secondly, a stability analysis is required to rigorously define the range of applicability of the present numerical technique. Finally, the method must be extended to three-dimensional configurations in order to investigate more realistically the propagation of mechanical waves in heterogeneous media.

ACKNOWLEDGMENTS

This work was performed under the Project SAC000D04-High-Resolution Low-Frequency Synthetic Aperture Sonar (HRLFSAS) of the STO-CMRE Programme of Work, funded by the NATO Allied Command Transformation.

REFERENCES

- ¹Finn B. Jensen, William A. Kuperman, Michael B. Porter, and Henrik Schmidt. Computational Ocean Acoustics. Springer New York, New York, NY, 2011.
- ²M. Bruneau. Equations of Motion in Dissipative Fluid. John Wiley & Sons, Ltd, 2010. ISBN 9780470612439.
- ³Allan D. Pierce. The Wave Theory of Sound. Springer International Publishing, Cham, 2019. ISBN 978-3-030-11214-1.
- ⁴W. M. Ewing, W. S. Jardetzky, and F. Press. Fundamental Equations and Solutions. New York: McGraw-Hill, 1957.
- ⁵R. Sabatini, O. Marsden, C. Bailly, and O. Gainville. Three-dimensional direct numerical simulation of infrasound propagation in the Earth’s atmosphere. Journal of Fluid Mechanics, 859:754–789, 2019.

- ⁶Julien Berland, Christophe Bogey, Olivier Marsden, and Christophe Bailly. High-order, low dispersive and low dissipative explicit schemes for multiple-scale and boundary problems. Journal of Computational Physics, 224(2):637 – 662, 2007. ISSN 0021-9991.
- ⁷Christophe Bogey and Christophe Bailly. A family of low dispersive and low dissipative explicit schemes for flow and noise computations. J. Comput. Phys., 194(1):194–214, 2004. ISSN 0021-9991.
- ⁸Dimitri Komatitsch, Christophe Barnes, and Jeroen Tromp. Wave propagation near a fluid-solid interface: A spectral-element approach. GEOPHYSICS, 65(2):623–631, 2000.
- ⁹Mario Zampolli, Alessandra Tesei, Finn B. Jensen, Nils Malm, and John B. Blottman. A computationally efficient finite element model with perfectly matched layers applied to scattering from axially symmetric objects. The Journal of the Acoustical Society of America, 122(3):1472–1485, 2007.
- ¹⁰M. Zampolli, A. L. Espana, K. L. Williams, S. G. Kargl, E. I. Thorsos, J. L. Lopes, Jermaine L. Kennedy, and P. L. Marston. Low- to mid-frequency scattering from elastic objects on a sand sea floor: Simulation of frequency and aspect dependent structural echoes. Journal of Computational Acoustics, 20(02):1240007, 2012.
- ¹¹Paul Cristini and Dimitri Komatitsch. Some illustrative examples of the use of a spectral-element method in ocean acoustics. The Journal of the Acoustical Society of America, 131(3):EL229–EL235, 2012.
- ¹²Influence of the sediment characteristics and of the level of burial on the acoustic response of a hollow cylinder in shallow water, 2019.
- ¹³Numerical simulation of full-wave propagation in the time domain : an useful tool for underwater acoustic applications, 2019.
- ¹⁴Bruno Lombard and Joël Piraux. Numerical treatment of two-dimensional interfaces for acoustic and elastic waves. Journal of Computational Physics, 195(1):90 – 116, 2004. ISSN 0021-9991.
- ¹⁵Francis Collino, Patrick Joly, and Florence Millot. Fictitious domain method for unsteady problems:. Journal of Computational Physics, 138(2):907 – 938, 1997. ISSN 0021-9991.
- ¹⁶Chaoming Zhang and Randall J. LeVeque. The immersed interface method for acoustic wave equations with discontinuous coefficients. Wave Motion, 25(3):237 – 263, 1997. ISSN 0165-2125.
- ¹⁷J. Farzi and S. M. Hosseini. High order immersed interface method for acoustic wave equation with discontinuous coefficients. Iranian Journal of Numerical Analysis and Optimization, 4:1–24, 2014.
- ¹⁸Joël Piraux and Bruno Lombard. A new interface method for hyperbolic problems with discontinuous coefficients: One-dimensional acoustic example. Journal of Computational Physics, 168(1):227 – 248, 2001. ISSN 0021-9991.
- ¹⁹Bruno Lombard and Joël Piraux. Numerical modeling of elastic waves across imperfect contacts. SIAM Journal on Scientific Computing, 28(1):172–205, 2006.

- ²⁰B. Lombard, J. Piraux, C. Gélis, and J. Virieux. Free and smooth boundaries in 2-D finite-difference schemes for transient elastic waves. Geophysical Journal International, 172(1):252–261, 2008. ISSN 0956-540X.
- ²¹Bruno Lombard and Joël Piraux. Numerical modeling of transient two-dimensional viscoelastic waves. Journal of Computational Physics, 230(15):6099 – 6114, 2011. ISSN 0021-9991.
- ²²Guillaume Chiavassa and Bruno Lombard. Time domain numerical modeling of wave propagation in 2-D heterogeneous porous media. Journal of Computational Physics, 230(13):5288 – 5309, 2011. ISSN 0021-9991.
- ²³David S. Abraham, Alexandre Noll Marques, and Jean-Christophe Nave. A correction function method for the wave equation with interface jump conditions. Journal of Computational Physics, 353:281 – 299, 2018. ISSN 0021-9991.
- ²⁴Roberto Sabatini and Paul Cristini. An immersed interface method for the solution of the standard parabolic equation in range-dependent ocean environments. The Journal of the Acoustical Society of America, 143(4):EL243–EL247, 2018.
- ²⁵Raghav Singhal and Jiten C Kalita. A novel higher order compact-immersed interface approach for elliptic problems. Physics of Fluids, 33(8), 2021.
- ²⁶Raghav Singhal and Jiten C Kalita. An efficient explicit jump high-order compact immersed interface approach for transient incompressible viscous flows. Physics of Fluids, 34(10), 2022.
- ²⁷Bertil Gustafsson. The convergence rate for difference approximations to mixed initial boundary value problems. Mathematics of Computation, 29(130):396–406, 1975. ISSN 00255718, 10886842.
- ²⁸E. F. Toro, R. C. Millington, and L. A. M. Nejad. Towards Very High Order Godunov Schemes. Springer US, Boston, MA, 2001. ISBN 978-1-4615-0663-8.
- ²⁹Thomas Schwartzkopff, Michael Dumbser, and Claus-Dieter Munz. Fast high order ADER schemes for linear hyperbolic equations. Journal of Computational Physics, 197(2):532 – 539, 2004. ISSN 0021-9991.
- ³⁰Egon Krause, Yurii Shokin, Michael Resch, and Nina Shokina, editors. Arbitrary high order finite volume schemes for linear wave propagation, Berlin, Heidelberg, 2006. Springer Berlin Heidelberg. ISBN 978-3-540-31768-5.
- ³¹Bruno Lombard. Modélisation numérique de la propagation et de la diffraction d’ondes mécaniques. Habilitation à Diriger des Recherches de l’Université d’Aix-Marseille 2, 2010.
- ³²Bruno Lombard. Méthodes numériques pour la propagation des ondes mécaniques et acoustiques en présence d’interfaces. PhD thesis, Université d’Aix-Marseille 2, 2002.
- ³³J. R. Barber. Stress Function Formulation. Springer Netherlands, Dordrecht, 2010. ISBN 978-90-481-3809-8.
- ³⁴Michael Hardy. Combinatorics of partial derivatives. The Electronic Journal of Combinatorics, 13:1 – 13, 2006.

- ³⁵A. Mennucci. An intuitive presentation of faà di bruno’s formula, 2017. Convegno. L’eredità matematica e civile di Francesco Faà di Bruno. Politecnico di Torino, 22 settembre 2017.
- ³⁶F. Faà di Bruno. Sullo sviluppo di funzioni. Annali di Scienze matematiche e Fisiche, 6: 479–480, 1855.
- ³⁷R. L. Mishkov. Generalization of the formula of faà di bruno for a composite function with a vector argument. International Journal of Mathematics and Mathematical Sciences, 24: 498526, 1999. ISSN 0161-1712.
- ³⁸Christopher K.W. Tam and Jay C. Webb. Dispersion-relation-preserving finite difference schemes for computational acoustics. Journal of Computational Physics, 107(2):262 – 281, 1993. ISSN 0021-9991.
- ³⁹Alexander B Baynes. Scattering of low-frequency sound by compact objects in underwater waveguides. Technical report, Naval Postgraduate School, 2018.
- ⁴⁰Roberto Sabatini, Yan Pailhas, Angeliki Xenaki, Alessandro Monti, and Paul Cristini. Far-field analytical solutions of the non-homogeneous helmholtz and wave equations for spatially non-localized sources. JASA Express Letters, 3(2):022401, 2023.